

Quantum Mechanical Limits on Beam Demagnification and Luminosity

F. Zimmermann, CERN, Geneva, Switzerland

Abstract

Quantum-mechanical limits on the final focusing and the ultimate luminosity are reviewed, including the minimum spot size, the maximum phase-space density, Oide effect, and beamstrahlung.

1 INTRODUCTION

Quantum mechanics introduces limits on the spot size and luminosity achievable in an electron-positron linear collider. The most fundamental constraints arise from the uncertainty principle and the Fermi-Dirac statistics. Others are due to the quantum fluctuations of synchrotron radiation or beamstrahlung and pair creation during the beam-beam collision.

In this report we investigate the minimum spot size and ultimate luminosity permitted by quantum mechanics, and study how close to this limit presently proposed linear-collider designs are. Specifically, we address the minimum spot size, the maximum phase-space density, the effect of synchrotron radiation in the final quadrupoles (Oide limit), the constraints due to beamstrahlung, and the ultimate luminosity.

For the purpose of illustration, we consider parameters for three different linear collider designs — TESLA, NLC, and CLIC —, for which we assume the parameters listed in Table 1.

2 DIFFRACTION LIMITED SPOT SIZE

We can derive the quantum limit by a simple analogy between a classical beam, light, and a quantum particle [1]. For a classical particle beam the variation of the rms beam size near the collision point is described by

$$\sigma_y(s) = \sqrt{\epsilon_y \left(\beta_y^* + \frac{s^2}{\beta_y^*} \right)}, \quad (1)$$

where β_y^* denotes the beta function at the collision point, s the longitudinal distance from this point, and ϵ_y the geometric beam emittance.

For a light beam or laser pulse an analogous expression applies,

$$\sigma_y^\gamma(s) = \sqrt{\frac{\lambda}{4\pi} \left(Z_R + \frac{s^2}{Z_R} \right)}, \quad (2)$$

where Z_R , the Rayleigh length, is the equivalent of the beta function, and $\lambda/4$ the equivalent of the geometric beam emittance.

The equation for a single quantum particle is

$$\sigma_y^{QM}(s) = \sqrt{\frac{\lambda_e}{2\gamma} \left(\beta_y^* + \frac{s^2}{\beta_y^*} \right)}, \quad (3)$$

where β_y^* is the same as the classical beta function. As for the laser, the emittance of the beam is replaced by the particle's (quantum) wave length λ_e/γ , divided by 4π .

Comparison of (1) and (3) shows that the quantum mechanical limit is reached, when the normalized emittance approaches the value $\lambda_e/2 \approx 0.2$ pm. This normalized emittance is still 4 to 5 orders of magnitude smaller than the damping-ring target emittances.

Inserting the limiting emittance, we find a minimum spot size of 5–30 pm for all three projects of Table 1.

3 BEAM DESCRIPTION BY WIGNER DISTRIBUTION

Instead of using the wave function $\phi(x)$ for computing quantum effects in an accelerator, it appears more convenient to employ the equivalent description in terms of a Wigner distribution. The Wigner distribution is defined as [2]

$$W(x, p) = \frac{1}{\hbar} \int_{-\infty}^{\infty} \exp\left(\frac{i}{\hbar}py\right) \phi\left(x - \frac{y}{2}\right) \phi^*\left(x + \frac{y}{2}\right) dy.$$

For an uncorrelated Gaussian wave packet with centroid position x_0 and centroid momentum p_0 , the function W is

$$W(x, p, x_0, p_0) = \frac{1}{2\pi\sigma_x\sigma_p} \exp\left(-\frac{1}{2} \left[\frac{(x-x_0)^2}{\sigma_x^2} + \frac{(p-p_0)^2}{\sigma_p^2} \right]\right),$$

where $\sigma_x\sigma_p = \hbar/2$. It is tempting to identify W with the classical particle density. Indeed, if the two are initially identical, in a linear system they remain the same for all times. The temporal evolution of $W(x, p, t)$ is described by the Wigner-Moyal equation, which for linear or quadratic potentials reduces to the classical Liouville equation. However, for a general wave function ϕ , or a nonlinear system W is not a positive function, and, thus, it differs from the classical density. A non-negative quantum-mechanical distribution is available in the form of the Husimi function [3], which corresponds to a 'smoothed' Wigner distribution.

In the early 1990s, R. Fedele and coworkers have applied the quantum dynamical formalism to describe classical particle transport, by introducing the 'thermal wave model' [4]. Instead of demonstrating the similarity of the

Table 1: Parameters for future linear collider projects

parameter	symbol	TESLA	NLC	CLIC
bunch population [10^{10}]	N_b	2	0.8	0.4
DR energy [GeV]	E_{DR}	5	1.98	2.42
emittance from DR [nm]	$\gamma\epsilon_{x,y,DR}$	8000, 20	3000, 30	620, 5
DR bunch length [mm]	σ_z	6	3.6	1.2
DR energy spread [10^{-3}]	σ_E/E	1	0.9	1.1
DR beta [m]	$\beta_{y,DR}$	60	4	4
FF emittance [nm]	$\gamma\epsilon_{x,y,FF}$	10000, 30	3600, 40	680, 10
IP beam energy [GeV]	E^*	250	250	1500
IP beta [mm]	$\beta_{x,y}^*$	15, 0.4	8, 0.11	6, 0.07
IP spot size w/o pinch [nm]	$\sigma_{x,y}^*$	554, 5.0	243, 3.0	67, 0.7
free length from IP [m]	l^*	3.0	3.5	4.3
Upsilon	Υ	0.05	0.13	8.3
BS photons / e^-	N_γ	1.56	1.26	2.32

quantum description and the classical description, it might be worthwhile to focus on the differences, and to determine under which conditions quantum effects will become visible in the linear-collider beam transport.

For example, since in a nonlinear system the time evolution of the Wigner distribution is different from that of the classical distribution, we may ask whether the strong sextupoles in the final focus could give rise to quantum-mechanical deviations from the classical behavior.

4 PHASE SPACE DENSITY

Due to Pauli's exclusion principle, each phase space unit volume of dimension h^3 can accommodate only one polarized electron. Attributing a phase-space area of $2\pi\epsilon$ to each plane of motion (ϵ is the geometric emittance in that plane), this gives rise to the phase-space density limit

$$\rho_{ps} \equiv \frac{N}{\gamma^3 \epsilon_x \epsilon_y \epsilon_z} \leq \frac{1}{\lambda_e^3}. \quad (4)$$

Table 2 shows that actual damping-ring design parameters are still far away from this limit thanks, in particular, to the huge longitudinal emittance.

Table 2: Design densities and quantum-mechanical limits for various damping rings.

parameter	symbol	TESLA	NLC	CLIC
density [m^{-3}]	ρ_{ps}	2×10^{23}	7×10^{23}	2×10^{25}
limit [m^{-3}]	$1/\lambda_e^3$	7×10^{34}	7×10^{34}	7×10^{34}

5 SYNCHROTRON RADIATION IN THE FINAL QUADRUPOLE (OIDE EFFECT)

If electrons (or positrons) emit synchrotron radiation photons when traversing the final quadrupole(s), they lose energy and acquire a different focal length, as illustrated in

Fig. 1. Since the photon emission is a random process, this leads to an unavoidable blow up of the collision-point spot size. The blow up becomes larger as the IP beta functions are squeezed to smaller values, due to larger particle amplitudes and hence magnetic fields in the quadrupole.

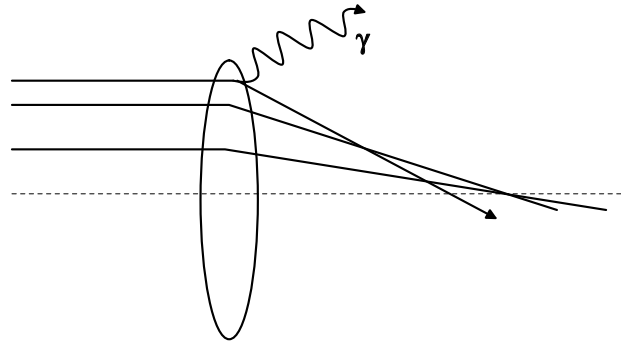


Figure 1: Schematic of Oide effect; particles emitting synchrotron radiation in the final quadrupole are no longer focused at the collision point.

The effect was first analyzed by K. Oide [5] and is therefore known as the 'Oide effect'. Subsequently, the impact on the luminosity was studied in a joint paper by K. Hirata, B. Zotter, and K. Oide [6].

The total number of photons emitted per electron in the final quadrupole,

$$N \approx \frac{5}{2\sqrt{3}} \alpha \gamma \theta \approx \frac{5}{2\sqrt{3}} \alpha \gamma K l^* \sqrt{\frac{\epsilon_y}{\beta_y^*}}, \quad (5)$$

is of the order of 1 (α is the fine-structure constant), indicating that the beam distribution at the interaction point (IP) is non-Gaussian. The energy loss per unit length in the final quadrupole is

$$\frac{d\delta}{ds} \approx \frac{2}{3} r_e \gamma^3 \frac{K^2 l^{*2} \epsilon_y}{\beta_y^*}, \quad (6)$$

and the change in relative energy squared per unit length (a quantum effect)

$$\frac{d\delta^2}{ds} \approx \frac{55}{24} r_e \lambda_e \gamma^5 \frac{K^3 l^{*3} \epsilon_y^{3/2}}{\beta_y^{*3/2}}. \quad (7)$$

The collision point spot size can be expressed as

$$\sigma_y^{*2} = \beta_y^* \epsilon_y + \frac{110}{3\sqrt{6\pi}} r_e \lambda_e \gamma^5 F(K_q, L_q, l^*) \left(\frac{\epsilon_y}{\beta_y^*} \right)^{5/2}, \quad (8)$$

where

$$F(K_q, L_q, l^*) = \int_0^{\sqrt{K_q L_q}} |\sin \phi + \sqrt{K_q} l^* \cos \phi|^3 \left[\int_0^\phi (\sin \phi' + \sqrt{K_q} l^* \cos \phi')^2 d\phi' \right]^2 d\phi, \quad (9)$$

L_q is the length of the quadrupole, K_q its strength (in units of m^{-2}), and l^* the free length between the exit face of the quadrupole and the IP.

Figure 2 is a graphical illustration of Eq. (8). The upper curve corresponds to the CLIC design emittance (at the entrance of the final focus), the other to a 100 times smaller value. The figure shows that the CLIC beam size can be reduced significantly by further lowering the emittance, but not by decreasing the beta function below the actual design value $\beta_y^* \approx 70 \mu\text{m}$ [7]. In Fig. 2, we have chosen $F = 5.4$, which refers to the CLIC final focus [7], but the result is quite insensitive to the precise value of F .

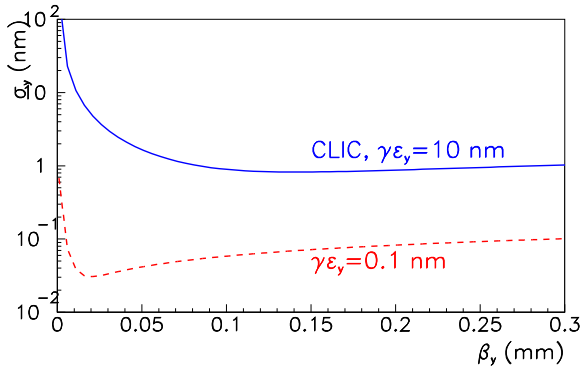


Figure 2: Vertical IP spot size σ_y^* , Eq. (8), as a function of the IP beta function, for a normalized emittance of 10 nm, and a 100 times smaller emittance, and assuming $F \approx 5.4$ (value for the CLIC final focus).

The rms beam size is minimum for [5]

$$\beta_y^* = \left(\frac{275}{3\sqrt{6\pi}} r_e \lambda_e F(K_q, L_q, l^*) \right)^{2/7} \gamma (\gamma \epsilon_y)^{3/7}, \quad (10)$$

suggesting that, near the Oide limit, the IP beta function increases linearly with energy, which may hinder the desired increases in luminosity at ultra-high energies.

Inserting the optimum value of β_y^* , the minimum IP spot size is obtained as [5]

$$\sigma_{y\min}^* = \left(\frac{7}{5} \right)^{1/2} \left(\frac{275}{3\sqrt{6\pi}} r_e \lambda_e F(K_q, L_q, l^*) \right)^{1/7} (\gamma \epsilon_y)^{5/7}. \quad (11)$$

It is independent of energy, but depends on the normalized emittance, and, weakly, on the function F .

Figure 3 shows the minimum spot size (11) as a function of the normalized emittance. For the smallest emittance allowed by quantum mechanics, $\gamma \epsilon_y \approx \lambda_e/2$, the minimum spot size becomes 1.3 pm. We consider this value as the ultimate quantum-mechanical limit for the present type of final-focus systems. Fortunately it is still three orders of magnitude away from present designs.

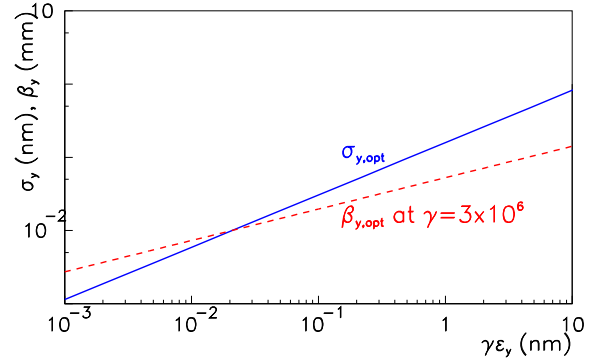


Figure 3: Minimum IP spot size $\sigma_{y\min}^*$, Eq. (11), as a function of the normalized emittance, assuming $F \approx 5.4$.

6 SYNCHROTRON RADIATION IN DETECTOR SOLENOID FIELD, WITH CROSSING ANGLE

An effect similar to the Oide effect arises from synchrotron radiation emitted in the fringe and body of the detector solenoid, especially if the beams collide under a crossing angle. The energy loss of the particle, together with the vertical dispersion generated by the horizontal component of the solenoid field (due to the crossing angle), leads to a blow up of the spot size at the collision point.

The effect of synchrotron radiation in the solenoid body was computed analytically by J. Irwin [8]:

$$\begin{aligned} \frac{\Delta \sigma_y^{*2}}{\sigma_y^{*2}} &= \frac{c_u r_e \lambda_e \gamma^5}{\sigma_y^{*2}} \int ds R_{36}(s)^2 \left| \frac{1}{\rho(s)} \right|^3 \\ &= \frac{1}{20} \frac{c_u r_e \lambda_e}{\sigma_y^{*2}} \left(\frac{B_s \theta_{cl} l^* \gamma}{2B\rho} \right)^5. \end{aligned} \quad (12)$$

A larger effect can arise from the fringe field of the solenoid. This is illustrated in Figs. 4 and 5, simulation examples for CLIC, which show the dependence of the vertical blow up on the crossing angle, on the solenoid field and on the longitudinal extent of the fringe.

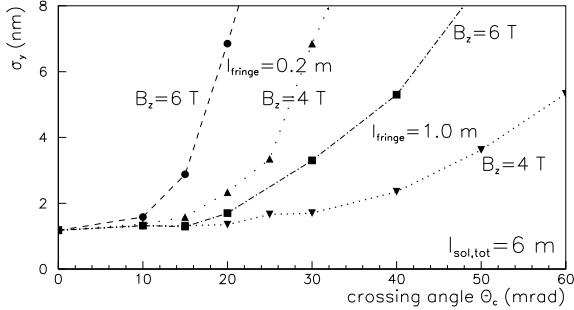


Figure 4: Simulated vertical spot size σ_y^* at the CLIC collision point vs. θ_c considering solenoid fields of 4 and 6 T [9].

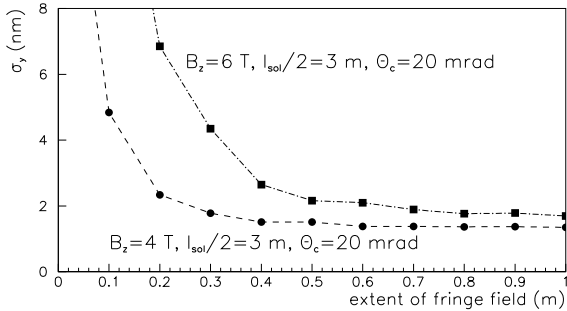


Figure 5: Simulated vertical spot size σ_y^* at the CLIC collision point vs. length of the fringe field (right), considering solenoid fields of 4 and 6 T [9].

7 POSSIBLE REMEDIES FOR THE OIDE EFFECT

A number of approaches could help to reduce, alleviate, or overcome the minimum spot size set by the Oide effect:

- Properly taking into account the photon statistics and computing the actual luminosity, K. Hirata, B. Zotter and K. Oide found that the rms spot size overestimates the luminosity loss [6].
- The average strength of the quadrupoles can be adjusted (tapered or lowered) so as to compensate for the effect of the average energy loss.

- Octupoles installed near the final quadrupole can even compensate the average energy loss as a function of amplitude [10].
- The synchrotron radiation is suppressed, if $\rho/\gamma \gg \beta$ [11], where ρ/γ represents the radiation formation length and ρ the local bending radius.
- The radiation is also suppressed for an ‘ultra-dense’ beam, due to Pauli’s exclusion principle.
- Smaller emittances allow for smaller spot sizes.
- An adiabatic focuser can overcome the Oide limit, and may allow for much smaller spot sizes.

In the following, we discuss the last option in detail.

8 ADIABATIC FOCUSER

The concept of an adiabatic focuser was proposed by P. Chen, K. Oide, A.M. Sessler and S.S. Yu in 1990 [12], as a measure to bypass the Oide limit.

In adiabatic focusing the quadrupole gradient is continuously increasing in the direction of beam propagation. In parallel, the beta function (or beam size) are continually decreasing, and particle amplitudes are limited by an envelope function that is also decreasing. The amplitude of a lower energy particle will never exceed that of the reference particle at nominal energy. For the concept of the adiabatic focuser it is important that this statement holds true, even if a particle loses energy due to synchrotron radiation. In this way the Oide limit can be overcome. Figure 6 displays a schematic of the adiabatic focuser. We note that the term ‘adiabatic’ refers to the condition that the change in β occurring over a length β is small compared with β .

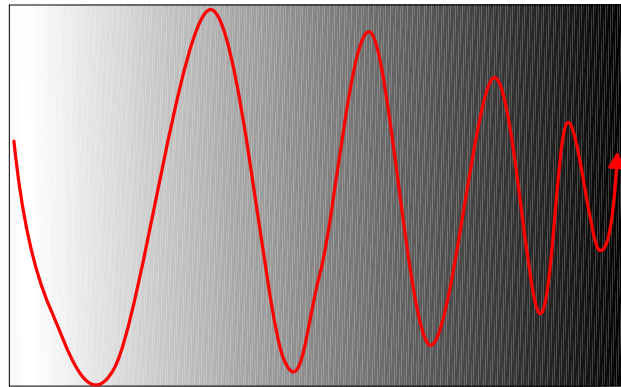


Figure 6: Schematic of adiabatic focuser. The varying shade indicates the increasing focusing gradient.

For simplicity, Ref. [6] has considered the special case of constant $\alpha(s) = \alpha_0$ (where $\alpha(s) = -(d\beta/ds)/2$), such that

$$K(s) = \frac{1 + \alpha_0^2}{\beta(s)^2}, \quad (13)$$

i.e., the focusing strength increases with s as $1/\beta^2$.

One distinguishes three different regimes of energy loss: classical synchrotron radiation, transition regime, and the quantum regime, depending on the value of $\Upsilon = \gamma^2 \lambda_e / \rho$ (here ρ is taken to be the local bending radius at an amplitude equal to the rms beam size). The energy loss per unit length in these three cases is

$$\frac{d\gamma}{ds} = -\frac{2}{3} \frac{\alpha}{\lambda_e} \times \begin{cases} \Upsilon^2, & \text{for } \Upsilon \leq 0.2 \text{ (classical)} \\ 0.2\Upsilon, & \text{for } 0.2 \leq \Upsilon \leq 22 \text{ (trans.)} \\ 0.556\Upsilon^{2/3}, & \text{for } 22 \leq \Upsilon \text{ (quantum)} \end{cases} \quad (14)$$

where α denotes the fine-structure constant, and γ the relativistic Lorentz factor.

The limitation on the adiabatic focusing arises from the average fractional energy loss, which should be much less than unity. This imposes a lower limit on the beta function. For the classical regime, the resulting numerical value for the minimum spot size is comparable to the Oide limit, although the origin of the latter is different (the stochastic nature of the radiation). Thus, to overcome the value of the Oide limit with an adiabatic focuser we must enter the transition or quantum regimes.

Combining the requirement that $\Delta\gamma/\gamma \ll 1$ with an optical matching condition between two regimes, one finds that a certain normalized emittance $\gamma\epsilon$ is required for passing from the classical into the transition regime, namely [12]

$$\gamma\epsilon \ll \gamma\epsilon_{\text{trans}} \equiv \frac{5^4 6 \lambda_e}{\alpha} \frac{\alpha_0^3}{(1 + \alpha_0^2)^2}. \quad (15)$$

Similarly, for entering the quantum regime, an even smaller emittance is needed [12]:

$$\gamma\epsilon \ll \gamma\epsilon_{\text{quant}} \equiv \frac{15^3}{2^3 4^2 22} \frac{\lambda_e}{\alpha} \frac{\alpha_0^3}{(1 + \alpha_0^2)^2}. \quad (16)$$

The expression on the right-hand side assumes a maximum value for $\alpha_0 = \sqrt{3}$. The corresponding ‘critical’ emittance to reach the quantum regime is

$$\gamma\epsilon_{\text{quant}} = \frac{3^{3/2} 15^3}{2^3 4^2 22} \lambda_e \alpha^3 \approx 6.2 \times 10^{-6} \text{ m}. \quad (17)$$

We note that the condition $\epsilon \ll \epsilon_{\text{quant}}$ is already met by most future linear-collider proposals.

In the quantum regime, the minimum spot size becomes [12]

$$\sigma_{y_{\text{min,AF}}}^* = \left(\frac{2}{11} \lambda_e (\gamma\epsilon_y)^2 \right)^{1/3} \exp \left(-3 \left(\frac{3^{3/2}}{16} \frac{\lambda_e}{\alpha^3 \gamma \epsilon_y} \right)^{1/2} \right). \quad (18)$$

Equation (18) promises extremely small spot sizes, as illustrated in Fig. 7. For $\gamma\epsilon_y = 10$ nm, the adiabatic focuser could produce a spot size of 10^{-9} nm!

However, a major problem with this approach is the enormous gradient required. The authors of [12] assume

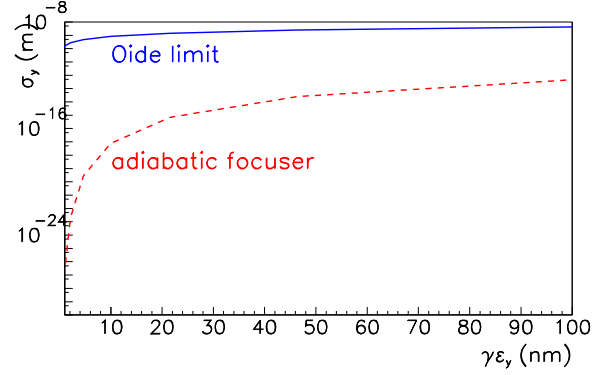


Figure 7: Minimum IP spot size $\sigma_{y_{\text{min,AF}}}^*$, Eq. (18), as a function of the normalized emittance.

that a tapered gradient is realized by a plasma of varying density. Then, the electron density of the (underdense) plasma is proportional to the quadrupole gradient K via

$$n_{\text{pl}} \approx \frac{\gamma K}{2\pi r_e}. \quad (19)$$

Figure 8 displays the final gradient (computed from Eq. (13) by inserting the minimum beta function due to energy loss considerations) and the equivalent plasma density according to (19) as a function of the normalized emittance (note the expanded horizontal scale). The densities range from 10^{23} cm^{-3} to 10^{30} cm^{-3} . For comparison, plasma densities in typical plasma wake-field acceleration experiments extend from about 10^{14} cm^{-3} to 10^{20} cm^{-3} [14], while metals, *e.g.*, copper, have a density of the order of 10^{23} molecules per cubic centimeter. This suggests that for most of the parameter range in Fig. 8 the ‘plasma’ would need to be denser than a solid.

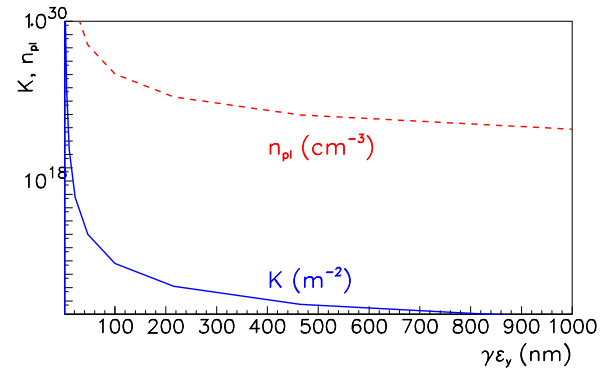


Figure 8: Final gradient K and the corresponding plasma density $n_{\text{pl}} \approx \gamma K / (2\pi r_e)$.

9 BEAMSTRAHLUNG AND ULTIMATE LUMINOSITY

As illustrated by a schematic in Fig. 9, during the collision the electrons (or positrons) are bent in the strong field of the opposing beam and emit synchrotron radiation. This radiation is called beamstrahlung. In order to reduce the beamstrahlung, while retaining a reasonable luminosity, the colliding beams are usually chosen as flat. The amount of beamstrahlung is then determined only by the bunch charge, the beam energy, the bunch length, and the horizontal spot size, but independent of the vertical spot size. Details of beam-beam phenomena in linear colliders can be found in the review by K. Yokoya and P. Chen [13].

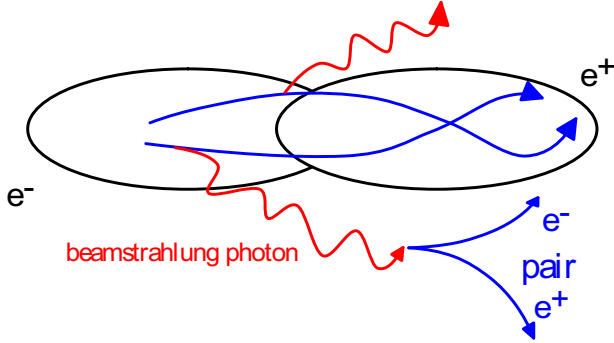


Figure 9: Illustration of beam-beam phenomena in a linear collider: beamstrahlung and pair production during the collision of electron and positron bunches.

The beamstrahlung implies two unwanted side effects. First, the luminosity spectrum is degraded, *i.e.*, not all the collision events occur at the nominal center-of-mass energy. Second, the beamstrahlung photons can convert into electron-positron pairs. If the beam fields are strong (small beam sizes) the pair production is coherent, *i.e.*, the conversion occurs in the coherent field of the opposing beam. Large numbers of particles are produced, which may cause background in the detector.

The character and the quantum nature of the beam-beam collision is determined by the average Upsilon parameter [13],

$$\Upsilon = \left\langle \frac{2\hbar\omega_c}{3E} \right\rangle \approx \frac{5}{6} \frac{\gamma r_e^2 N_b}{\alpha \sigma_z (\sigma_x + \sigma_y)}, \quad (20)$$

and by the number of beamstrahlung photons emitted per electron [13],

$$N_\gamma \approx \frac{5\alpha\sigma_z}{2\gamma\lambda_e} \frac{\Upsilon}{(1 + \Upsilon^{2/3})^{1/2}} \approx 2 \frac{\alpha r_e N_b}{\sigma_x + \sigma_y}, \quad (21)$$

where α denotes the fine-structure constant, and the last approximation applies if $\Upsilon \leq 1$.

The fraction of the luminosity at the design center-of-mass energy, $\Delta L/L$, is directly related to N_γ via [8]

$$\Delta\mathcal{L}/\mathcal{L} \approx 1/N_\gamma^2 (1 - e^{-N_\gamma})^2, \quad (22)$$

and the average energy loss of an electron during the collision can be expressed in terms of N_γ and Υ as [13]

$$\delta_B \approx \frac{1}{2} N_\gamma \Upsilon \frac{(1 + \Upsilon^{2/3})^{1/2}}{(1 + (1.5\Upsilon)^{2/3})^2}. \quad (23)$$

We next rewrite the luminosity equation as follows [15]:

$$L = \frac{f_{\text{rep}} n_b N_b^2}{4\pi \sigma_x^* \sigma_y^*} = \frac{1}{4\pi} \frac{P_{\text{wall}} \eta}{E_b} \frac{N_b}{\sigma_x^* \sigma_y^*}, \quad (24)$$

where $\eta = P_{\text{beam}}/P_{\text{wall}} = f_{\text{rep}} N_b n_b / P_{\text{wall}}$, f_{rep} is the repetition rate, P_{wall} the wall plug power, P_{beam} the beam power, η the efficiency of converting wall-plug power into beam power, and E_b the beam energy.

In order to discover new physics at high energies, the luminosity should increase (at least) as the square of the beam energy [16], because most cross sections decrease as $1/\gamma^2$.

We can derive two different estimates for the ultimate luminosity including the basic quantum constraints.

First, we ignore both beamstrahlung and Oide effect, and assume that all three emittances are quantum limited. Specifically, we suppose that $\gamma\epsilon_{y,z} \approx \lambda_e/2$, $\gamma\epsilon_x \approx N_b \lambda_e/2$, $\beta_{x,y}^* \approx \sigma_z$, and

$$\sigma_z \approx \frac{\gamma\epsilon_z}{\gamma(\Delta p/p)_{\text{rms}}},$$

where, *e.g.*, the relative momentum spread $(\Delta p/p)_{\text{rms}}$ may correspond to the rms bandwidth of the final focus (typically about 0.0028). Inserting these relations into (24), the luminosity becomes

$$L_1 = \frac{1}{4\pi} \frac{P_{\text{wall}} \eta}{E_b \sqrt{N_b}} \frac{4\gamma^2}{\lambda_e^2} (\Delta p/p)_{\text{rms}}. \quad (25)$$

The luminosity increases as the square of the energy, and, hence, in this case there is no quantum limit for the maximum energy.

In the second case we maintain a constant value of N_γ , in order not to dilute the luminosity spectrum. Hence, in this case we assume $N_\gamma \approx \text{const.}$ (this constrains N_b/σ_x), $\gamma\epsilon_{y,z} \approx \lambda_e/2$, $\beta_y^* \approx \sigma_z$, $\sigma_z \approx (\gamma\epsilon_z)/\gamma/(\Delta p/p)_{\text{rms}}$. For $\Upsilon \leq 1$ the luminosity becomes

$$L_{2,a} \approx \frac{1}{8\pi} \frac{P_{\text{wall}} \eta N_\gamma}{E_b} \frac{2\gamma}{r_e^2} \sqrt{(\Delta p/p)_{\text{rms}}}, \quad (26)$$

and, for $\Upsilon \gg 1$,

$$L_{2,b} \approx \frac{3}{20\pi} \frac{P_{\text{wall}} \eta}{E_b} \left(\frac{4N_\gamma}{5\alpha} \right)^{3/2} \frac{\alpha}{r_e^2} \gamma^2 \left(\frac{\Delta p}{p} \right)_{\text{rms}}. \quad (27)$$

Thus, confining the number of beamstrahlung photons, the luminosity raises either linearly with energy (for small Υ) or again quadratically (for large Υ). The luminosities (26) or (27) should be lower than (25), the latter being the more fundamental limit. A computed limit (27) higher than (25)

is an indication that keeping a constant value of N_γ is impossible, but that the latter is bound to decrease due to the minimum phase-space volume occupied by the beam.

From the above relations, we can compute the potential luminosity increases over the present design values which are permitted by quantum mechanics. For the first case, the factor of potential luminosity improvement is

$$H_{L,1} = \frac{L_1}{L_{\text{design}}} \approx \frac{4\gamma^2}{\lambda_e^2 \sqrt{N_b}} \sigma_{x,\text{des}}^* \sigma_{y,\text{des}}^* \left(\frac{\Delta p}{p} \right)_{\text{rms}},$$

where $\sigma_{x,\text{des}}^*$ and $\sigma_{y,\text{des}}^*$ are the design spot sizes. For the second case and $\Upsilon \leq 1$, we find

$$H_{L,2a} = \frac{L_2}{L_{\text{design}}} \approx \frac{\gamma \sigma_{y,\text{des}}^* \sigma_{x,\text{des}}^* N_\gamma}{r_e^2 N_b} \left(\frac{\Delta p}{p} \right)_{\text{rms}}^{1/2},$$

whereas, for $\Upsilon \gg 1$,

$$H_{L,2b} = \frac{L_2}{L_{\text{design}}} \approx \frac{6\alpha \sigma_{x,\text{des}}^* \sigma_{y,\text{des}}^*}{5r_e^2 N_b} \left(\frac{4N_\gamma}{5\alpha} \right)^{3/2} \gamma^2 \left(\frac{\Delta p}{p} \right)_{\text{rms}}.$$

Table 3 shows the luminosity enhancement factors $H_{L,1}$, $H_{L,2a}$, and $H_{L,2b}$ for various projects at their present design energy. The table also lists the extrapolated energy reach, which is computed by requiring that the luminosity increases as the square of the energy, again considering the three different cases. The energy limit in case 2a exceeds the Planck energy (1.2×10^{19} GeV). A similar result was first obtained by J. Irwin in 1996 [17]. The other two cases allow for increases in energy (and luminosity) without limit. Alternative scaling laws for luminosity and beamstrahlung were discussed in Refs. [18, 19].

10 CONCLUSIONS

The quantum nature of electrons allows focusing the beam spot sizes down to about 1 pm. An ultimate limit on the emittance arises from the uncertainty principle and a limit on the beta function from synchrotron radiation in the final quadrupole ('Oide effect').

According to fundamental constraints (uncertainty and exclusion principles) and ignoring the Oide effect, but keeping the number of beamstrahlung photons per electron constant, the Planck scale can be reached with a luminosity that increases as the square of the energy ($L \propto \gamma^2$), if we extrapolate from the present 1-TeV designs.

The performance of these designs is, however, already constrained by Oide effect, beamstrahlung, and, in particular, the available beam emittances. Thus, even though the fundamental quantum mechanical limits are still distant,

new optics concepts and approaches will be needed for producing, focusing and colliding beams with spot sizes below 1 nm.

11 ACKNOWLEDGEMENTS

I thank Ralph Assmann for suggesting this presentation. Also, I am grateful to Francesco Ruggiero and John Jowett for helpful discussions, and to Gilbert Guignard for a careful reading of the manuscript.

12 REFERENCES

- [1] K.-J. Kim, "Introduction to Working Group A: Quantum Fluctuations in Beam Dynamics," presented at Advanced ICFA Beam Dynamics Workshop on Quantum Aspects in Beam Physics, Capri, 2000.
- [2] S. Brandt, H.D. Dahmen, "The Picture Book of Quantum Mechanics," 2nd edition, Springer Verlag, New York.
- [3] K. Husimi, Proc. Phys. Math. Soc. Japan **22**, 264 (1940).
- [4] R. Fedele and G. Miele, Nuovo Cimento D **13** (1991) p. 1527
- [5] K. Oide, "Synchrotron-Radiation Limit on the Focusing of Electron Beam," Phys. Rev. Letters **61** (1988) p. 1713
- [6] K. Hirata, B. Zotter, K. Oide, "Synchrotron Radiation Limit of the Luminosity in TeV Linear Colliders," Physics Letters B **224** (1989) p. 437
- [7] F. Zimmermann et al., these proceedings.
- [8] C. Adolphsen et al., "Zeroth Order Design Report for the Next Linear Collider", presented at Snowmass '96, *LBNL-5424, SLAC-474, UCRL-ID-124161, UC-414* (1996).
- [9] D. Schulte, F. Zimmermann, "The Crossing Angle in CLIC," Proc. PAC'2001 Chicago, USA, CERN/PS 2001-038 (AE), CLIC Note 484, and CERN-SL-2001-043 (AP) (2001).
- [10] P. Raimondi, private communication (2001).
- [11] R. Ruth, "Fundamental Aspects of Low Emittance Electron Beams," presented at Advanced ICFA Beam Dynamics Workshop on Quantum Aspects in Beam Physics, Capri, 2000.
- [12] P. Chen, K. Oide, A.M. Sessler, S.S. Yu, "Plasma-Based Adiabatic Focuser," Phys. Rev. Letters **64** (1990) p. 1231
- [13] K. Yokoya, P. Chen, "Beam-Beam Phenomena in Linear Colliders," Lecture at 1990 US-CERN School on Particle Accelerators, Hilton Head Island, So. Carolina, published by Springer-Verlag (1990).
- [14] R. Assmann, "Review of Ultrahigh Gradient Acceleration Schemes, Review of Experiments," EPAC 2002, Paris (2002).
- [15] R. Brinkmann, private communication (1992).
- [16] J. Ellis, "Particle Physics at Future Colliders," this workshop.
- [17] J. Irwin, private communication, Snowmass 1996 (1996).
- [18] R.B. Palmer, "Prospects for High Energy e^+e^- Linear Colliders," Ann. Rev. Nucl. Part. Sci. **40** (1990) p. 529
- [19] J.P. Delahaye, G. Guignard, T. Raubenheimer, and I. Wilson, "Scaling Laws for e^+e^- Linear Colliders," CLIC Note 533 (1997).

Table 3: Factors of potential luminosity increase permitted by quantum constraints, and the estimated energy reach, if the luminosity increases as the square of the energy, without any other constraints (case 1) or keeping the number of beamstrahlung photons constant either for a low or a high value of Υ (cases 2a and 2b). The Lorentz factor γ_0 refers to the design beam energy listed in Table 1. The numbers in parentheses do not apply, either because they correspond to a low- Υ scaling for a high- Υ design — or vice versa —, or because the more fundamental limit (25) sets a tighter limit.

parameter	symbol	TESLA	NLC	CLIC
case 1 for $\gamma = \gamma_0$	$H_{L,1}$	9×10^{12}	4×10^{12}	1×10^{13}
energy reach		∞	∞	∞
case 2a for $\gamma = \gamma_0$	$H_{L,2a}$	7×10^8	4×10^8	(5×10^8)
energy reach [GeV]		1.8×10^{20}	9.5×10^{19}	(8.1×10^{20})
case 2b for $\gamma = \gamma_0$	$H_{L,2b}$	(2×10^{14})	(1×10^{14})	(1×10^{15})
energy reach [GeV]		(∞)	(∞)	∞